Geometric Tracking Control of Aerial Robots Based on Centroid Vectoring

Lovro Marković, Antun Ivanović, Marko Car, Matko Orsag, Stjepan Bogdan

***Abstract*— This paper focuses on presenting the concept of geometric tracking control for an unmanned aerial vehicle (UAV) based on variations in center of gravity (CoG). The proposed UAV model has the ability to exploit its dynamic CoG as a means of stabilization and control. A mathematical model of such a system is used as a base for developing the nonlinear geometric tracking controller on the special Euclidean group SE(3). Finally, two unique UAV models, presented with a trajectory tracking problem, are simulated in a realistic simulation environment. Performance of the selected control terms is analyzed based on relevant simulation results.**

I. INTRODUCTION

Multirotor UAVs have been a topic of great research interest over the course of past decade. The first mathematical model of quadrotor vehicle capable of vertical takeoff and landing has been presented in [1]. Since then, researchers have been working on various control designs, payload transportation and attaching manipulators on such vehicles. This research allowed UAVs to execute various tasks and interact with the environment. However, the common denominator in all that research is treating the payload and movement of the manipulator as a disturbance. Such approach puts all the effort for canceling these effects on controller. Although we are used to treating these effects as disturbances, a question arises: why don't we use them to our advantage? This underdog idea has not reached much attention in research community and it is one of the greatest motivators for this paper. The main goal is to develop a geometric controller capable of utilizing manipulator movement in order to track attitude.

Geometric control concept is well known in aerial robotics community, and has previously been applied for classic quadrotor vehicles in [2], [3], [4]. The UAV is considered to be in plus configuration and the CoG coincides with the body of the UAV. Furthermore, the model of the UAV is augmented with the CoG dynamics so we can exploit manipulator movement for attitude tracking. In our previous work we designed and implemented the Moving Mass Control concept (MMC) [5]. In that paper we use a standard quadrotor UAV with mounted moving masses on the arms of the UAV while the control structure uses standard PID blocks. This is a novel concept first developed in [6] with attitude control considered in [7]. Up to this point, nonlinear geometric control has not been applied to the moving-mass controlled UAV.

Authors are with Faculty of Electrical and Computer Engineering, University of Zagreb, 10000 Zagreb, Croatia (Antun Ivanović, Marko Car, Tomislav Haus, Matko Orsag, Stjepan Bogdan, Lovro Marković) at fer.hr

Aside from aforementioned linear cartesian manipulator, we consider achieving CoG variations with planar manipulator. The envisioned scenario is payload transportation with such a manipulator where any displacement in the payload creates variations in CoG. UAVs endowed with manipulators have previously been studied in [8], [9]. Similar problem has already been presented in [10] where end-effector trajectory tracking of a single mounted 3-DOF manipulator is considered. However, in this paper, along with the different approach in controller synthesis, two 2-DOF manipulators are used, each carrying a payload. The main subject for trajectory tracking is still the UAV, while manipulators are considered as an extension, used only for attitude control.

Therefore, contributions of this paper are: to derive the appropriate dynamic model for UAVs with variable CoG on the SE(3) configuration manifold; choose control terms based on that model; and evaluate controller performance on a predefined trajectory tracking problem using two unique UAV models described previously.

The paper is organized as follows. In Section II we present the generalized mathematical model on the SE(3) configuration manifold, along with expressions for CoG and moments of inertia. Based on that mathematical model, Section II shows how to obtain the proper control terms to achieve desirable error dynamics alongside sufficient stability conditions. In Section IV we conduct two sets of simulations using Gazebo and ROS environment by executing the same trajectory for different UAVs. Finally, the conclusions are drawn in Section V.

II. Mathematical model

First of all, it is necessary to introduce a fixed inertial reference frame $\{\mathbf{e}_1, \mathbf{e}_2, \mathbf{e}_3\}$ and a body-fixed frame $\{\mathbf{b}_1, \mathbf{b}_2, \mathbf{b}_3\}$. Next, we present a general equation for calculating CoG vector from the origin of the body-fixed frame as follows:

$$\mathbf{r}_{CoG} = \frac{m_b \mathbf{r}_b + \sum_{i=1}^{n} m_i \mathbf{r}_i}{m_b + \sum_{i=1}^{n} m_i} = \frac{\sum_{i=1}^{n} m_i \mathbf{r}_i}{m_t}, \qquad (1)$$

The following terms are defined as:

- $\mathbf{r}_{CoG} \in \mathrm{R}^3$ - CoG with respect to the body-fixed frame
- $\mathbf{r}_i \in \mathrm{R}^3$ - Position of the i-th mass or payload w.r.t. the body-fixed frame
- $\mathbf{r}_b \in \mathrm{R}^3$ - Position of UAV body w.r.t. the body-fixed frame. Note that because the body frame origin coincides with the rigid body CoG (without considering the moving masses) this term yields $\mathbf{r}_b = 0_{3x1}$
- $m_b \in \mathbb{R}$ - Mass of the UAV body
- $m_i \in \mathbb{R}$ - Mass of the i-th moving mass or payload
- $m_t \in \mathbb{R}$ - Mass of the whole UAV system

Moment of inertia matrix expressed in the body-fixed frame is defined as follows:

$$\mathrm{J} = \mathrm{J}_b + \sum_{i=1}^{n} \mathrm{J}_i \,, \tag{2}$$

where $\mathrm{J}_b \in \mathbb{R}^3$ is body and $\mathrm{J}_i \in \mathbb{R}^3$ is the moment of inertia of some mass element outside the origin of the body-fixed frame. Using the parallel axis theorem, one is able to calculate J_i while knowing the moment of inertia around its CoG:

$$\mathrm{J}_i = \mathrm{J}_{i,CoG} + m_i(\mathbf{r}_i^T \cdot \mathbf{r}_i \mathrm{I}_{3\times 3} - \mathbf{r}_i \cdot \mathbf{r}_i^T) \tag{3}$$

Now we can express the equations of motion in the inertial frame while taking in consideration CoG vector which is located outside the origin of the body-fixed frame[11].
It is important to note that the changes in the moment of inertia and CoG have been omitted in favor of simplicity in equations (5) and (7). The complete model dynamics expressed in the inertial frame are presented in V.

$$\dot{\mathbf{x}} = \mathbf{v} \tag{4}$$

$$m_t\dot{\mathbf{v}} + m_t g\mathbf{e}_3 - m_t \mathrm{R}\mathbf{r}_{CoG} \times \dot{\mathbf{\Omega}} - m_t \mathrm{R}\hat{\mathbf{\Omega}}\hat{\mathbf{r}}_{CoG}\mathbf{\Omega} = f\mathrm{R}\mathbf{e}_3 \tag{5}$$

$$\dot{\mathrm{R}} = \mathrm{R}\hat{\mathbf{\Omega}} \tag{6}$$

$$\mathrm{J}\dot{\mathbf{\Omega}} + \mathbf{\Omega} \times \mathrm{J}\mathbf{\Omega} + m_t \mathbf{r}_{CoG} \times \mathrm{R}^T\dot{\mathbf{v}} = \mathbf{M} \tag{7}$$

The *hat map* is an operator equivalent to the expression $\hat{\mathbf{x}}\mathbf{y} = \mathbf{x} \times \mathbf{y}$. It maps elements of $\mathbb{R}^3$ to the so(3) Lie algebra.
The following terms are defined as:

- $\mathrm{J} \in \mathbb{R}^{3\times 3}$ - Moment of inertia matrix w.r.t. the body-fixed frame
- $\mathrm{R} \in SO(3)$ - Rotation matrix from the body fixed frame to the inertial frame
- $\mathbf{\Omega} \in \mathbb{R}^3$ - Angular velocity in the body-fixed frame
- $\mathbf{x} \in \mathbb{R}^3$ - Location of the body-fixed frame in the inertial frame
- $\mathbf{v} \in \mathbb{R}^3$ - Velocity of the body-fixed frame in the inertial frame
- $f \in \mathbb{R}$ - Total thrust produced by the UAV
- $\mathbf{M} \in \mathbb{R}^3$ - Total moments acting in the body-fixed frame

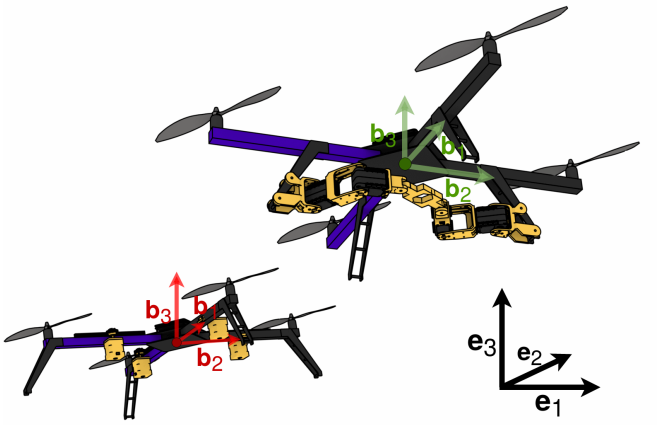

Fig. 1: UAV model with MMC (left) and two 2-DOF overactuated manipulators (right) along with their respective coordinate systems. The manipulator end effectors are placed diametrically opposite from each other.

Equations (4), (5), (6) and (7) describe the dynamical flow of a rotating and translating rigid body in terms of evolution of $(\mathrm{R}, \mathbf{x}, \mathbf{\Omega}, \dot{\mathbf{x}}) \in \mathrm{TSE}(3)$ on the tangent bundle of SE(3).

Height and yaw of the UAV is controlled with variations in rotor velocity, whereas roll and pitch with variations in CoG. It is assumed that the first and the third propeller rotate clockwise, while the second and the fourth rotate counter-clockwise. The relation between moments, thrust and rotor velocity is the following:

$$f_i = b_f \omega_i^2 \tag{8}$$

$$\tau_i = (-1)^i b_m f_i \,, \tag{9}$$

where the following terms are defined as:

- $f_i \in \mathbb{R}$ - Thrust of the i-th motor
- $\tau_i \in \mathbb{R}$ - Moment i-th motor produces
- $b_f \in \mathbb{R}$ - Motor thrust constant
- $b_m \in \mathbb{R}$ - Motor moment constant
- $\omega_i \in \mathbb{R}$ - Rotation velocity of the i-th rotor

Total thrust can be expressed as:

$$f = \sum_{1}^{4} f_i \,, \tag{10}$$

and total moment acting in the body-fixed frame as:

$$\begin{aligned} \mathbf{M} = [&m_p g d_x \mathbf{e}_1 \cdot \mathbf{b}_{3,d}, \\ &m_p g d_y \mathbf{e}_2 \cdot \mathbf{b}_{3,d}, \\ &b_m(-f_1 + f_2 - f_3 + f_4)] \,, \end{aligned} \tag{11}$$

where $d_x \in \mathbb{R}$ and $d_y \in \mathbb{R}$ are moving mass or payload offsets along x and y axis respectively.
Using (10) and (11) as control inputs of the system one is able to obtain the desired force of each rotor and the control offsets d_x and d_y. While the control offsets are able to be directly applied as moving mass control inputs, in the manipulator case an additional transformation needs

to take place.
Both manipulators are overactuated, meaning they have three actuators while operating in a 2-DOF workspace. They are placed in a diametrically opposite configuration as seen in 1, therefore only a single set of infinitesimal angle increments $\Delta q_1, \Delta q_2, \Delta q_3$ is sufficient as control input for both manipulators.
Conversion from payload offsets to angle increments is done using the inverse Jacobian of the manipulator end effector. Direct Jacobian matrix is presented as follows:

$$\begin{bmatrix} d_x \\ d_y \end{bmatrix} = \mathcal{J}(q_1, q_2, q_3) \cdot \begin{bmatrix} \Delta q_1 \\ \Delta q_2 \\ \Delta q_3 \end{bmatrix} \tag{12}$$

$$\mathcal{J} = \begin{bmatrix} l_1 \cos(q_1) & l_2 \cos(q_1 + q_2) & l_3 \cos(q_1 + q_2 + q_3) \\ l_1 \sin(q_1) & l_2 \sin(q_1 + q_2) & l_3 \sin(q_1 + q_2 + q_3) \end{bmatrix}, \tag{13}$$

where l_1, l_2 and l_3 are the manipulator link lengths, while q_1, q_2 and q_3 are current actuator angles. Using Jacobian pseudoinverse, incremental update rule for actuator angles can be obtained as follows:

$$\begin{bmatrix} \Delta q_1 \\ \Delta q_2 \\ \Delta q_3 \end{bmatrix} = \mathcal{J}^{-1}(q_1, q_2, q_3) \cdot \begin{bmatrix} d_x \\ d_y \end{bmatrix} \tag{14}$$

Manipulator and moving mass actuator dynamics along with the change in desired rotor force is regarded as instantaneous while presenting the controller synthesis and stability conditions. However, within the Gazebo simulation environment, a certain transfer dynamic is taken into account.

III. Geometric control on SE(3)

The main focus of the proposed controller is put on position tracking. Therefore, the trajectory consists of a desired position $\mathbf{x}_d(t)$ and a desired heading $\mathbf{b}_{1,d}(t)$ of the body-fixed frame. Since the given position is known ahead of time, one is able to calculate both desired linear velocity $\mathbf{v}_d(t)$ and acceleration $\mathbf{a}_d(t)$ which are also inherently included as inputs.
The controller is developed on the nonlinear Lie group SE(3) consisting of the rotation group SO(3) and translation group T(3). It is cascade in structure, as seen in 2 with position tracking block following attitude tracking block. The main advantage of using the SO(3) rotation group is to avoid any singularities or ambiguities that may arise when representing rotations with Euler angles or quaternions.
Controller synthesis is carried out as follows. First, position and orientation tracking errors are presented as the proportional and derivative part of the controller. In addition, nonlinear control terms are chosen to compensate proposed model dynamics. Finally, exponential stability conditions for the initial UAV configuration are shown.

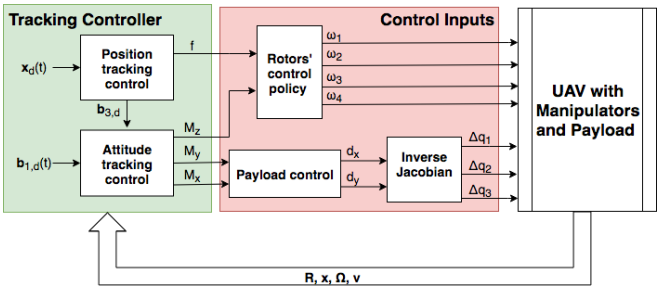

Fig. 2: Control scheme for the UAV carrying a payload. When considering UAV with MMC *Inverse Jacobian* block becomes the identity matrix. This means that the control inputs d_x and d_y are directly sent as system inputs.

A. Tracking errors

Compatible attitude error function and transport map between tangent bundles of SO(3) are chosen as suggested in [12] and confirmed in research regarding geometric control with aerial vehicles [4], [13], [3], [2]. Attitude error function on SO(3) $\Psi(\mathrm{R}, \mathrm{R}_d)$ along with its compatible transport map $\mathcal{T}(\mathrm{R}, \mathrm{R}_d)$ are chosen as:

$$\Psi(\mathrm{R}, \mathrm{R}_d) = \frac{1}{2} tr[I - \mathrm{R}_d^T \mathrm{R}] \tag{15}$$

$$\mathcal{T}(\mathrm{R}, \mathrm{R}_d) = \mathrm{R}^T \mathrm{R}_d \tag{16}$$

Linear position and velocity tracking errors are defined as follows:

$$\mathbf{e}_x = \mathbf{x} - \mathbf{x}_d \tag{17}$$

$$\mathbf{e}_v = \mathbf{v} - \mathbf{v}_d \tag{18}$$

It is shown in [12] that the attitude tracking error should be chosen as a left-differential of the attitude error function $\Psi(\mathrm{R}, \mathrm{R}_d)$ as follows:

$$\mathbf{e}_\mathrm{R} = \frac{1}{2} (\mathrm{R}_d^T \mathrm{R} - \mathrm{R}^T \mathrm{R}_d)^\vee \tag{19}$$

Due to the fact that angular velocities $\mathbf{\Omega} \in T_\mathrm{R} SO(3)$ and $\mathbf{\Omega}_d \in T_{\mathrm{R}_d} SO(3)$ evolve in different tangential bundles, the proposed left transport map (16) needs to be applied when calculating the angular velocity tracking error:

$$\mathbf{e}_\Omega = \mathbf{\Omega} - \mathrm{R}^T \mathrm{R}_d \mathbf{\Omega}_d \tag{20}$$

B. Control terms

After defining all tracking errors, one can start constructing the control terms. Taking in consideration the proposed system dynamics (5) and (7), the force and moment control terms are chosen as follows:

$$\begin{aligned} \mathbf{A} =& (-\mathrm{k}_x \mathbf{e}_x - \mathrm{k}_v \mathbf{e}_v \\ &+ mg\mathbf{e}_3 + m\ddot{\mathbf{x}}_d \\ &- m\mathrm{R}\mathbf{r}_{CoG} \times \dot{\mathbf{\Omega}} - m\mathrm{R}\hat{\mathbf{\Omega}}\hat{\mathbf{r}}_{CoG}\mathbf{\Omega}) \\ f =& \mathbf{A} \cdot \mathrm{R}\mathbf{e}_3 \end{aligned} \tag{21}$$

$$\begin{aligned}\mathbf{M} = &-\mathrm{k_R}\mathbf{e_R} - \mathrm{k_\Omega}\mathbf{e_\Omega} \\ &+\boldsymbol{\Omega}\times \mathrm{J}\boldsymbol{\Omega} - \mathrm{J}(\hat{\boldsymbol{\Omega}}\mathrm{R}^T\mathrm{R}_d\boldsymbol{\Omega}_d - \mathrm{R}^T\mathrm{R}_d\dot{\boldsymbol{\Omega}}_d) \\ &+m\mathbf{r}_{CoG}\times \mathrm{R}^T\ddot{\mathbf{x}}\end{aligned} \tag{22}$$

Desired rotation matrix is constructed in the conventional way when considering geometric control of aerial vehicles [2], [3], [13]. The proposed desired rotation matrix is constructed as $\mathrm{R}_d = [\mathbf{b}_{1,c}, \mathbf{b}_{3,d}\times\mathbf{b}_{1,c}, \mathbf{b}_{3,d}]$ where component vectors of R_d are calculated in the following way:

$$\mathbf{b}_{3,d} = \frac{\mathbf{A}}{||\mathbf{A}||} \tag{23}$$

$$\mathbf{b}_{1,c} = -\frac{(\mathbf{b}_{3,d}\times(\mathbf{b}_{3,d}\times\mathbf{b}_{1,d}))}{||\mathbf{b}_{3,d}\times\mathbf{b}_{1,d}||} \tag{24}$$

The chosen constraint for the trajectory tracking problem differ slightly from the one proposed in [2]. Due to the fact that model dynamics which include variable CoG are considered in this paper, new trajectory constraints are presented as follows:

$$||mge_3 + m\ddot{\mathbf{x}}_d - m\mathrm{R}\mathbf{r}_{CoG}\times\dot{\boldsymbol{\Omega}} - m\mathrm{R}\hat{\boldsymbol{\Omega}}\hat{\mathbf{r}}_{CoG}\boldsymbol{\Omega}|| < B\,, \tag{25}$$

where B is some positive constant.

Desired angular velocity and acceleration also need to be considered in this trajectory tracking problem. One is able to calculate the desired angular velocity and acceleration using R_d and its derivatives in the following way:

$$\hat{\boldsymbol{\Omega}}_d = \mathrm{R}_d^T\dot{\mathrm{R}}_d \tag{26}$$

$$\dot{\hat{\boldsymbol{\Omega}}}_d = -\hat{\boldsymbol{\Omega}}_d\hat{\boldsymbol{\Omega}}_d + \mathrm{R}_d^T\ddot{\mathrm{R}}_d \tag{27}$$

Derivatives of R_d are calculated using the backwards differentiation method. Another important note is that the computation rate of the desired angular velocity and acceleration is slower than the overall simulation rate. For further implementation details, please refer to [14].

lovro: Preformulirana rečenica: "Another important..."

C. Error dynamics

In order to express error dynamics, one needs to calculate the time derivatives of linear (18) and angular (20) tracking errors:

$$\mathbf{e}_v = \dot{\mathbf{x}} - \dot{\mathbf{x}}_d \tag{28}$$

$$\mathbf{e}_\Omega = \dot{\boldsymbol{\Omega}} + \hat{\boldsymbol{\Omega}}\mathrm{R}^T\mathrm{R}_d\boldsymbol{\Omega}_d - \mathrm{R}^T\mathrm{R}_d\dot{\boldsymbol{\Omega}}_d \tag{29}$$

After including (5) and (7) in (28) and (29) respectively, the following equations are obtained:

$$\begin{aligned}m\mathbf{e}_v = &-mg\mathbf{e}_3 - m\ddot{\mathbf{x}}_d \\ &+m\mathrm{R}\mathbf{r}_{CoG}\times\dot{\boldsymbol{\Omega}} + m\mathrm{R}\hat{\boldsymbol{\Omega}}\hat{\mathbf{r}}_{CoG}\boldsymbol{\Omega} \\ &+\mathbf{A} + \mathbf{X}\end{aligned} \tag{30}$$

$$\begin{aligned}\mathrm{J}\mathbf{e}_\Omega = &\mathbf{M} - \boldsymbol{\Omega}\times\mathrm{J}\boldsymbol{\Omega} \\ &+\mathrm{J}(\hat{\boldsymbol{\Omega}}\mathrm{R}^T\mathrm{R}_d\boldsymbol{\Omega}_d - \mathrm{R}^T\mathrm{R}_d\dot{\boldsymbol{\Omega}}_d) \\ &+m\mathbf{r}_{CoG}\times\mathrm{R}^T\ddot{\mathbf{x}}\end{aligned} \tag{31}$$

Note that in (30) $\mathbf{X}\in\mathrm{R}^3$ is a bounded term which equals:

$$\mathbf{X} = \frac{f}{(\mathrm{R}_d\mathbf{e}_3)^T\mathrm{R}\mathbf{e}_3}(\mathrm{R}_d\mathbf{e}_3 - ((\mathrm{R}_d\mathbf{e}_3)^T\mathrm{R}\mathbf{e}_3)\mathrm{R}\mathbf{e}_3) \tag{32}$$

After substituting control force from (21) and (22) in (30) and (31) respectively the final form of error dynamics is obtained:

$$m\mathbf{e}_v = -k_x\mathbf{e}_x - k_v\mathbf{e}_v + \mathbf{X} \tag{33}$$

$$\mathrm{J}\mathbf{e}_\Omega = -k_\mathrm{R}\mathbf{e}_\mathrm{R} - \mathrm{k}_\Omega\mathbf{e}_\Omega \tag{34}$$

D. Stability discussion

lovro: Ponovno napisan prvi odlomak

We begin by observing (33) and (34). It has to be taken in account that the derived error dynamics are identical to those presented in [4] and [2], even though the proposed model and control terms in this paper differ from previous research.
Therefore, to avoid redundancy, the complete stability proof is omitted for brevity. Instead, only final conclusions for attitude error function $\Psi(\mathrm{R}(t), \mathrm{R}_d(t))$ exponential asymptotic stability and tracking error attraction to the zero-equilibrium state are outlined as established in [4].

Granted the initial UAV configuration satisfies the following conditions:

$$\Psi(\mathrm{R}(0), \mathrm{R}_d(0)) < 2 \tag{35}$$

$$||\mathbf{e}_\Omega(0)||^2 < \frac{2}{\lambda_{min}(\mathrm{J})}k_\mathrm{R}(2 - \Psi(\mathrm{R}(0), \mathrm{R}_d(0))\,, \tag{36}$$

it can be shown that tracking errors of the whole system reaches zero-equilibrium state and the attitude function is exponentially bounded as:

$$\Psi(\mathrm{R}(t), \mathrm{R}_d(t)) \leq \min\{2, \alpha e^{-\beta t}\} \tag{37}$$

for some positive constants α and β.

IV. Simulation

Simulations are conducted in the Gazebo simulator within the ROS environment. UAV used in experiments is the μMorus which can be found in the *mmuav_gazebo* repository [14], along with its model parameters. Two experiments are conducted with UAVs using two different methods of CoG variation: MMC in the first case and payload carried by manipulators in the second case.
Control parameters for the first case are chosen as follows:

$$\mathrm{k}_x = \begin{bmatrix}10 & 0 & 0\\ 0 & 10 & 0\\ 0 & 0 & 50\end{bmatrix},\ \mathrm{k}_v = \begin{bmatrix}3.75 & 0 & 0\\ 0 & 3.75 & 0\\ 0 & 0 & 20\end{bmatrix},$$

$$\mathrm{k}_R = \begin{bmatrix}1.5 & 0 & 0\\ 0 & 1.5 & 0\\ 0 & 0 & 10\end{bmatrix},\ \mathrm{k}_\Omega = \begin{bmatrix}0.65 & 0 & 0\\ 0 & 0.65 & 0\\ 0 & 0 & 1.54\end{bmatrix},$$

Rotational control parameters, in the second case, stay the same, while translational parameters are the following:

$$k_x = \begin{bmatrix} 7.2 & 0 & 0 \\ 0 & 7.2 & 0 \\ 0 & 0 & 50 \end{bmatrix}, k_v = \begin{bmatrix} 2.6 & 0 & 0 \\ 0 & 2.6 & 0 \\ 0 & 0 & 20 \end{bmatrix},$$

For both cases, initial parameters are obtained by considering the error dynamics (33) and (34) in the equilibrium state. However, they are further tuned with better position tracking performance in mind.

how tuned?, lovro: for better position tracking

It is important to note that the actuator dynamics of moving masses and manipulators is taken in consideration within the Gazebo simulator. Furthermore there is a slight transient delay while increasing or decreasing rotor velocity which results in a non-instantaneous control force change.

The chosen trajectory tracking problem is formulated as a rotating spiral:

$$\mathbf{x}_d(t) = [0.4t;\ 0.5\sin(\pi t);\ 0.6\cos(\pi t) + 2]$$
$$\mathbf{b}_{1,d}(t) = [\cos\left(\frac{\pi}{5}t\right);\ \sin\left(\frac{\pi}{5}t\right);\ 0]$$

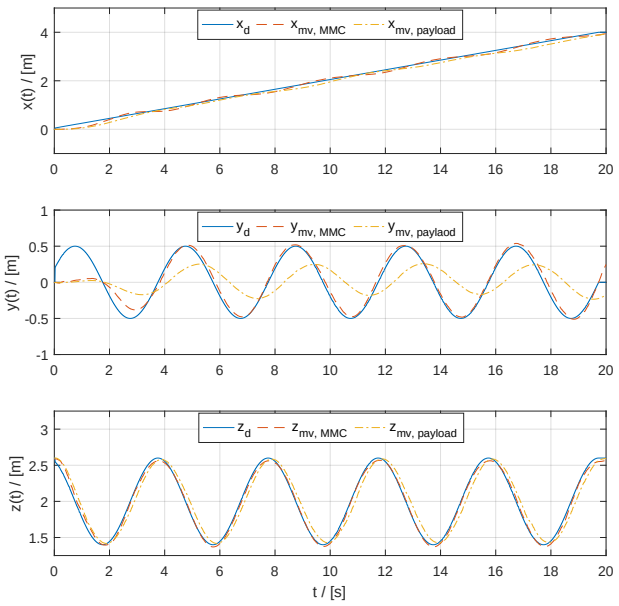

Fig. 3: Comparison between desired $\mathbf{x}_d$ and measured position values $\mathbf{x}_{mv}$ for both simulation cases. While tracking on x and z axes are reasonably similar, slower position tracking can be observed on the y axis for the second simulation case. Calculated MSE values are 0.0079 and 0.00352 for first and second case respectively.

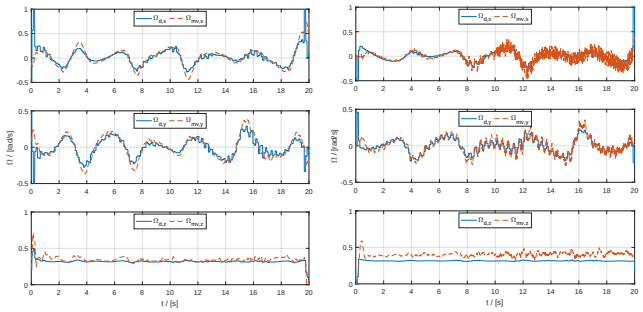

a) UAV with MMC b) UAV carrying a payload

Fig. 4: Comparison between desired $\mathbf{\Omega}_d$ and measured $\mathbf{\Omega}_{mv}$ angular velocities for both simulation cases. Better angular velocity tracking is achieved in the first case, while in the second case an oscillatory measured value is observed around x axis during later stages of trajectory tracking. It is interesting to note that although desired position and heading are the same for each case, a different desired angular velocity is obtained using (26).

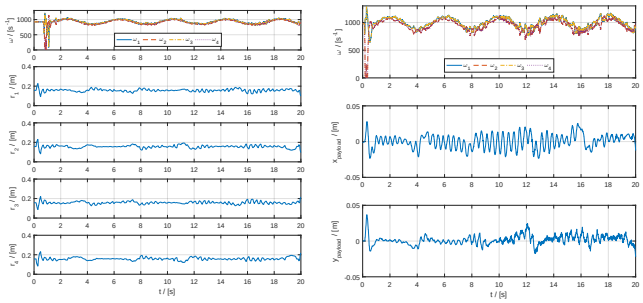

a) UAV with MMC b) UAV carrying a payload

Fig. 5: Figures show control inputs for both simulation cases: rotor velocities ω_i, moving mass and payload offsets r_i. Rotor velocities are similar because desired trajectory height is equal for both cases.

V. Conclusion

Geometric control was presented and implemented for two separate UAV models with variable centers of gravity. Although the controller has been constructed without actuator dynamics in mind, during the simulations its effect can be seen.

Moving mass actuator dynamics have a noticeably faster transient effect than the manipulator dynamics. This claim can be affirmed by observing 6 where variations in CoG produced by MMC occur quicker and achieve greater magnitudes than those produced by the carried payload. Therefore, it is expected that the UAV with MMC achieves better position and attitude tracking than UAV carrying a payload. In 3 it can be seen that this expectation is validated. In the first case(MMC) excellent tracking performance can be observed, while in the second case(payload) measured position along the y-axis exhibits

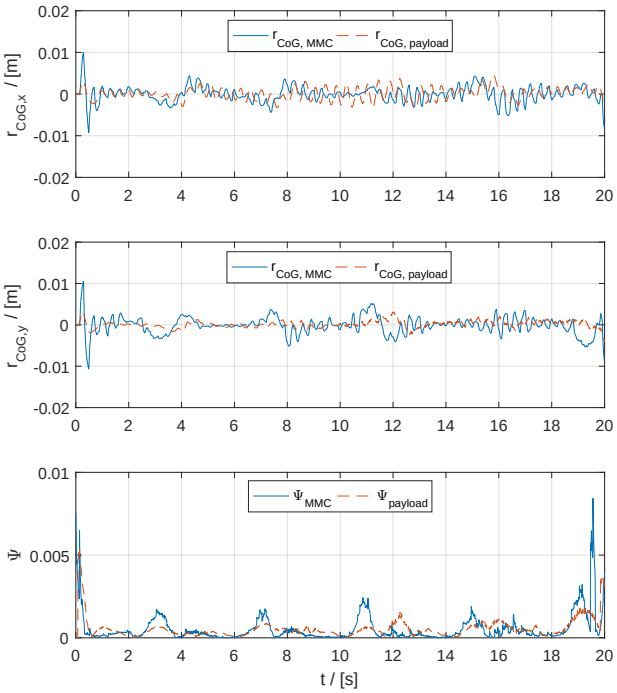

Fig. 6: Comparison between first two components of CoG vector $\mathbf{r}_{CoG}$ and between attitude error functions Ψ for both simulation cases. It can be seen that higher magnitude of CoG variation can be achieved using moving masses rather than the carried payload.

tracking delay and lower magnitude with respect to the desired position.
The overall effect of control terms 21 and 22 which include $\mathbf{r}_{CoG}$ becomes negligible if considering slower trajectories. In such cases, both UAVs can be observed as having CoG inside the origin of the body-fixed frame yielding simpler control terms.

APPENDIX

In this section rotating body dynamics with variations in center of gravity is derived. General form of Euler-Lagrange dynamics for a rotating rigid body in SE(3) configuration manifold in the body-fixed frame as presented in [11]:

$$\frac{d}{dt}\left(\frac{\partial \mathcal{L}}{\partial \mathbf{\Omega}}\right) + \mathbf{\Omega} \times \frac{\partial \mathcal{L}}{\partial \mathbf{\Omega}} + \mathbf{v} \times \frac{\partial \mathcal{L}}{\partial \mathbf{v}} + \sum_{i=1}^{3} \mathbf{r}_i \times \frac{\partial \mathcal{L}}{\partial \mathbf{r}_i} = 0 \tag{38}$$

$$\frac{d}{dt}\left(\frac{\partial \mathcal{L}}{\partial \mathbf{v}}\right) + \mathbf{\Omega} \times \frac{\partial \mathcal{L}}{\partial \mathbf{v}} - \mathrm{R}^T \frac{\partial \mathcal{L}}{\partial x} = 0 \tag{39}$$

For the the proposed UAV with variations in CoG the Lagrangian is:

$$\mathcal{L}(\mathrm{R}, x, \mathbf{\Omega}, \mathbf{v}) = \frac{1}{2}\mathbf{\Omega}^T J \mathbf{\Omega} + m\mathbf{\Omega}^T \hat{\mathbf{r}}_{cm}\mathbf{v} + \frac{1}{2} m \mathbf{v}^T \mathbf{v} - U(\mathrm{R}, \mathbf{x}), \tag{40}$$

where $U(\mathrm{R}, \mathbf{x})$ is the potential energy of the system. It is important to note that J and $\mathbf{r}_{cm}$ are variable over time. Lagrangian derivatives needed for the general form equations 38 and 39 are:

$$\frac{\partial \mathcal{L}}{\partial \mathbf{\Omega}} = J\mathbf{\Omega} + m\hat{\mathbf{r}}_{cm})\mathbf{v} \tag{41}$$

$$\frac{d}{dt}\left(\frac{\partial \mathcal{L}}{\partial \mathbf{\Omega}}\right) = \dot{J}\mathbf{\Omega} + J\dot{\mathbf{\Omega}} + m\dot{\mathbf{r}}_{cm} \times \mathbf{v} + m\mathbf{r}_{cm} \times \dot{\mathbf{v}} \tag{42}$$

$$\frac{\partial \mathcal{L}}{\partial \mathbf{v}} = m\mathbf{v} - m\mathbf{r}_{cm} \times \mathbf{\Omega} \tag{43}$$

$$\frac{d}{dt}\left(\frac{\partial \mathcal{L}}{\partial \mathbf{v}}\right) = m\dot{\mathbf{v}} - m\dot{\mathbf{r}}_{cm} \times \mathbf{\Omega} - m\mathbf{r}_{cm} \times \dot{\mathbf{\Omega}} \tag{44}$$

It is of interest to transfer rotation and translation dynamics in the inertial frame. This can be done using the following relations:

$$\mathbf{v} = \mathrm{R}^T \dot{x} \tag{45}$$

$$\dot{\mathbf{v}} = \mathrm{R}^T \ddot{\mathbf{x}} - \mathbf{\Omega} \times (\mathrm{R}^T \dot{\mathbf{x}}) \tag{46}$$

$$\mathbf{r}_{cm} = \mathrm{R}^T(\mathbf{x}_{cm} - \mathbf{x}) \tag{47}$$

$$\dot{\mathbf{r}}_{cm} = \mathrm{R}^T(\dot{\mathbf{x}}_{cm} - \dot{\mathbf{x}}) + \mathrm{R}^T \hat{\mathbf{\Omega}} \mathbf{x}_{cm} - \hat{\mathbf{\Omega}} \mathrm{R}^T(\mathbf{x}_{cm} - \mathbf{x}) \tag{48}$$

After plugging in 41, 42, 43, 44 in 38, 39 and using 45, 46 as transformations of velocity and acceleration to inertial frame the following equations are obtained:

$$\begin{aligned} &J\dot{\mathbf{\Omega}} + m\mathbf{r}_{cm} \times \mathrm{R}^T \ddot{\mathbf{x}} \\ &\quad + \dot{J}\mathbf{\Omega} + m\dot{\mathbf{r}}_{cm} \times \mathrm{R}^T \dot{\mathbf{x}} \\ &\quad + \mathbf{\Omega} \times J\mathbf{\Omega} + \sum_{i=1}^{3} \mathbf{r}_i \times \frac{\partial \mathcal{L}}{\partial \mathbf{r}_i} = 0 \end{aligned} \tag{49}$$

$$\begin{aligned} &m\ddot{\mathbf{x}} - m\mathrm{R}\hat{\mathbf{r}}_{cm}\dot{\mathbf{\Omega}} - m\mathrm{R}\hat{\mathbf{r}}_{cm}\mathbf{\Omega} \\ &\quad - m\mathrm{R}\hat{\mathbf{\Omega}}\hat{\mathbf{r}}_{cm}\mathbf{\Omega} + \frac{\partial U(\mathrm{R}, \mathbf{x})}{\partial \mathbf{x}} = 0 \end{aligned} \tag{50}$$

Finally, CoG transform 47, 48 is included along with forces and moments acting in the body-fixed frame and potential energy of the system which gives the following model dynamics:

$$\begin{aligned} &J\dot{\mathbf{\Omega}} + m\mathrm{R}^T(\mathbf{x}_{cm} - \mathbf{x}) \times \mathrm{R}^T \ddot{\mathbf{x}} + \dot{J}\mathbf{\Omega} \\ &\quad + m\widehat{\mathrm{R}^T \dot{\mathbf{x}}_{cm}} \mathrm{R}^T \dot{\mathbf{x}} - \mathrm{R}^T \dot{\mathbf{x}} \times (\mathrm{R}^T \hat{\mathbf{\Omega}} \mathbf{x}_{cm}) \\ &\quad - m\hat{\mathbf{\Omega}}\mathrm{R}^T(\mathbf{x}_{cm} - \mathbf{x}) \times \mathrm{R}^T \dot{\mathbf{x}} \\ &\quad + \mathbf{\Omega} \times J\mathbf{\Omega} = \mathbf{M} \end{aligned} \tag{51}$$

$$\begin{aligned} &m\ddot{\mathbf{x}} - m\mathrm{R}\widehat{\mathrm{R}^T(\mathbf{x}_{cm} - \mathbf{x})}\dot{\mathbf{\Omega}} \\ &\quad - m\mathrm{R}\widehat{\mathrm{R}^T(\dot{\mathbf{x}}_{cm} - \dot{\mathbf{x}})}\mathbf{\Omega} \\ &\quad - m\mathrm{R}\widehat{\mathrm{R}^T \hat{\mathbf{\Omega}} \mathbf{x}_{cm}}\mathbf{\Omega} \\ &\quad + mg\mathbf{e}_3 = f\mathrm{R}\mathbf{e}_3 \end{aligned} \tag{52}$$

ACKNOWLEDGMENT

This research was supported in part by NATO's Emerging Security Challenges Division in the framework of the Science for Peace and Security Programme as Multi Year Project under G. A. number 984807, named Unmanned system for maritime security and environmental monitoring - MORUS.

References

[1] T. Hamel, R. Mahony, R. Lozano, and J. Ostrowski, "Dynamic modelling and configuration stabilization for an x4-flyer," *IFAC Proceedings Volumes*, vol. 35, no. 1, pp. 217 – 222, 2002. 15th IFAC World Congress.

[2] T. Lee, M. Leok, and N. H. McClamroch, "Geometric tracking control of a quadrotor uav on se(3)," in *49th IEEE Conference on Decision and Control (CDC)*, pp. 5420–5425, Dec 2010.

[3] T. Lee, M. Leok, and N. Harris McClamroch, "Nonlinear Robust Tracking Control of a Quadrotor UAV on SE(3)," *ArXiv e-prints*, Sept. 2011.

[4] T. Lee, M. Leok, and N. Harris McClamroch, "Control of Complex Maneuvers for a Quadrotor UAV using Geometric Methods on SE(3)," *ArXiv e-prints*, Mar. 2010.

[5] T. Haus, M. Orsag, and S. Bogdan, "Design considerations for a large quadrotor with moving mass control," in *2016 International Conference on Unmanned Aircraft Systems (ICUAS)*, pp. 1327–1334, June 2016.

[6] T. Haus, M. Orsag, and S. Bogdan, "Mathematical modelling and control of an unmanned aerial vehicle with moving mass control concept," *Journal of Intelligent & Robotic Systems*, vol. 88, pp. 219–246, Dec 2017.

[7] T. Haus, N. Prkut, K. Borovina, B. Marić, M. Orsag, and S. Bogdan, "A novel concept of attitude control for large multirotor-uavs based on moving mass control," in *2016 24th Mediterranean Conference on Control and Automation (MED)*, pp. 832–839, June 2016.

[8] M. Orsag, C. Korpela, S. Bogdan, and P. Oh, "Dexterous aerial robots—mobile manipulation using unmanned aerial systems," *IEEE Transactions on Robotics*, vol. 33, pp. 1453–1466, Dec 2017.

[9] C. Korpela, M. Orsag, M. Pekala, and P. Oh, "Dynamic stability of a mobile manipulating unmanned aerial vehicle," in *2013 IEEE International Conference on Robotics and Automation*, pp. 4922–4927, May 2013.

[10] H. Yang and D. Lee, "Dynamics and control of quadrotor with robotic manipulator," in *2014 IEEE International Conference on Robotics and Automation (ICRA)*, pp. 5544–5549, May 2014.

[11] T. Lee, M. Leok, and N. H. McClamroch, *Global formulations of Lagrangian and Hamiltonian dynamics on manifolds : a geometric approach to modeling and analysis*. Interaction of mechanics and mathematics series, Springer, 2018.

[12] A. D. L. Francesco Bullo, *Geometric control of mechanical systems: modeling, analysis, and design for simple mechanical control systems*. Texts in applied mathematics 49, Springer, 1 ed., 2005.

[13] T. Fernando, J. Chandiramani, T. Lee, and H. Gutierrez, "Robust adaptive geometric tracking controls on so(3) with an application to the attitude dynamics of a quadrotor uav," in *2011 50th IEEE Conference on Decision and Control and European Control Conference*, pp. 7380–7385, Dec 2011.

[14] "mmuav gazebo." `https://github.com/larics/mmuav_gazebo/tree/geometry_control`, 2018.

[15] "Morus project." `http://www.fer.unizg.hr/morus`. Accessed: 2017-09-08.

[16] A. D. L. Francesco Bullo, *Geometric control of mechanical systems: modeling, analysis, and design for simple mechanical control systems*. Texts in applied mathematics 49, Springer, 1 ed., 2005.

[17] F. P. Schuller, *Lectures on the Geometric Anatomy of Theoretical Physics*. Friedrich-Alexander-Universität Erlangen-Nürnberg, Institut für Theoretische Physik III, 2017.